Schmidt hammer and terrestrial laser scanning (TLS) used to detect single event displacements on the Pleasant Valley fault (Nevada, USA)

Timothy Stahl[1] and Alexander Tye[2]

[1]Department of Geological Sciences, University of Canterbury, Christchurch, New Zealand

[2]Department of Earth and Environmental Sciences, University of Michigan, Ann Arbor, MI

KEYWORDS: Schmidt hammer, Paleoseismology, ~~Exposure age~~Fault scarp, ~~Limestone~~ ~~Scarp~~Terrestrial laser scanning,

Abstract

The surface roughness of carbonate fault scarps often reflect varying durations of exposure to subaerial weathering. On the Pleasant Valley fault in central Nevada, the documentation of a surface rupture in 1915, a long~~w~~ recurrence interval of faulting, slow weathering rate, and a relatively high (2-3 m) single event displacement make the discrimination of the historical and penultimate slip patches unambiguous. Following from a 2018 study, we used a Schmidt hammer and terrestrial laser scanning (TLS) to further test whether these weathering patterns delineate exposed slip patches on a fault scarp. Results show that Schmidt hammer rebound value ranges (termed ΔR – the difference between minimum and maximum R-values in repeat impacts at a point), increase by ~8-10 points across the historical-penultimate event transition zone in two separate scarp transects. TLS-derived surface roughness also indicates a clear difference between the most recent and penultimate events. The average single event displacement (SED) estimated using the Schmidt hammer and TLS is 2.85 m at two transect sites and is roughly equivalent to the visually estimated 3 m. While this fault is an ideal case where we know some of the slip history, the results demonstrate that these techniques show promise for discriminating slip patches on larger carbonate fault scarps with longer paleoearthquake histories, and could be used alongside ^{36}Cl cosmogenic exposure-age dating to improve paleoseismic records on normal faults.

This is the author manuscript accepted for publication and has undergone full peer review but has not been through the copyediting, typesetting, pagination and proofreading process, which may lead to differences between this version and the Version of Record. Please cite this article as doi: 10.1002/esp.4748

Introduction

Surface rupturing normal faults present a unique opportunity for identifying paleoearthquakes. Where normal faults rupture to the surface in bedrock, fault scarps – the surface expression of one or more earthquakes – may be preserved, allowing direct exposure-age dating of the fault surface and modelling of earthquake displacements and recurrence intervals (Bosi et al., 1993; Zreda and Noller, 1998). The use of cosmogenic ^{36}Cl on limestone scarps for these objectives is well-established and provides some of the most detailed paleoseismic records, with the best age precision, available on any fault (e.g., Zreda and Noller, 1998; Benedetti et al., 2002; Schlagenhauf et al., 2010; Benedetti and van der Woerd, 2014; Mouslopoulou et al., 2014; Mechernich et al., 2018). The difficulties associated with this technique are that it can be prohibitively time consuming and expensive to prepare and analyse samples at more than one scarp transect and at sampling intervals required to resolve event ages.

Relative age dating techniques, based primarily on rock weathering, have been used alongside ^{36}Cl exposure-age dating of fault scarps to corroborate results and guide sampling for cosmogenic nuclide dating (Stewart, 1996; Zreda and Noller, 1998; Giaccio et al., 2003; Tucker et al., 2011; Wei et al., 2013; Wiatr et al., 2015; He et al., 2016; Tye and Stahl, 2018). These techniques work on the premise that slip patches previously exposed in earthquakes have been subjected to a longer duration of subaerial weathering than more recently exposed patches. Wallace et al. (1984) was one of the first to recognise the potential for differential weathering and biogenic colonisation to yield relative age information on the Pleasant Valley scarp in central Nevada, USA. Based on relatively fresh limestone surfaces exposed in the moment magnitude (M_w) 6.9-7.0 1915 Pleasant Valley earthquake (Doser, 1988) compared to a higher, more deeply pitted patch, Wallace et al. (1984) proposed that the weathering pattern could be used to estimate the age of the pre-1915 most recent event (MRE) on the fault.

In this paper, we test the hypothesis of Wallace et al. (1984) on the Pleasant Valley fault using two techniques to characterise the differing degrees of weathering between the 1915 and pre-1915 slip patches. We begin first with a brief review of principles of relative-dating as applied to bedrock fault scarps, followed by a discussion of the study site and methods. We analyse Schmidt hammer rebound values (R-values) and terrestrial laser scanning (TLS) point clouds of the scarp face to characterise the near-surface weathering and roughening of the scarp over a single earthquake cycle. In doing so, we build on the methodology and results of Tye and Stahl (2018) from the Hebgen fault (Montana, USA) and provide unequivocal evidence that weathering contrasts in limestone slip patches are quantifiable under certain climatic and fault behaviour conditions (e.g., recurrence interval, RI, and single event displacement, SED). We conclude with recommendations for applying these techniques elsewhere.

Background

Relative age dating techniques

Relative-dating techniques were developed on the premise that time-dependent changes to rock masses and surfaces are quantifiable. One of the most widely-used applications is in exposure-age dating, where various metrics of surface weathering have been shown to correlate to the duration the rock surface has been exposed at or near the surface. Among other indicators, rock density and P-wave velocity (Maizel, 198~~7~~9; Crook and Gillespie, 1986); surface roughness (e.g., Wiatr et al., 2015; He et al., 2016), and pit depths (Tucker et al., 2011); weathering rind thickness and mineralogy (e.g., Laustela et al., 2003; Sak et al., 2004); and degree of lichen colonisation and lichen diameter (e.g. Benedict, 1985; Bull, 1996) all have been used as indicators of surface exposure age.

The Schmidt hammer tests rock hardness via a controlled impact of a spring-loaded piston against a surface and has been used in relative- and calibrated-age dating for years (c.f. Goudie, 2006). The distance that the piston rebounds within the device is measured and used to produce a rebound value (R-value). Larger R-values are generally expected from smoother and harder (or more elastic) rock surfaces. Schmidt hammer R-values have been shown to correlate with physical rock mass characteristics like uniaxial compressive strength (UCS) and Young's modulus of elasticity (E) (c.f. Goudie, 2006), as well as with time-dependent surface weathering characteristics like weathering rind thickness (Laustela et al., 2003; Stahl et al., 2013) and surface roughness (McCarroll, 1991; Tye and Stahl, 2018).

In order to interpret relative exposure ages from R-values, the user must control for other factors that influence R-value. Schmidt hammer R-values have been shown to be sensitive to variations in lithology (e.g., Goudie, 2006; Török et al., 2007), rock moisture content (Sumner and Nel, 2002), biologic weathering (Matthews and Owen, 2008), rock sample dimensions (Sumner and Nel, 2002; Aydin 2009; Demirdag et al., 2009), number of samples per surface (Niedzielski et al., 2009), operator bias (Shakesby et al., 2006), and instrument degradation (McCarroll 1987), among other factors. With adequate control for these factors, the largest influence on R-value is the duration of exposure at the surface.

In regions of tectonic extension, normal faults accommodate dilatational strain via brittle and ductile deformation. Under brittle deformation regimes, large earthquakes (> ~M_W 6) rupture normal faults at the ground surface, causing episodic, centimetre- to metre-scale discrete displacements (e.g. Nicol et al., 2006). Fault scarps in unconsolidated material form and subsequently erode, with the net vertical displacement across the degraded scarp indicating the cumulative displacement from all prior surface-rupturing earthquakes (e.g. Hanks et al., 1984). Fault scarps form and degrade in a different manner where normal faults rupture to the surface in competent bedrock (e.g., at range fronts). For example, in competent limestone lithologies, fault planes may be exposed and weather subaerially while maintaining the overall original scarp slope (e.g., Bosi et al., 1993). Limestone fault scarps therefore preserve horizontal (i.e., oriented along-strike) bands, or slip patches, with different exposure-ages corresponding to the timing of past earthquakes (e.g., Zreda and Noller, 1998; Giaccio et al., 2003). The different exposure ages may be reflected in rare earth element content (e.g. Manighetti et al., 2010; Mouslopoulou et al., 2011; Tesson et al., 2015) and/or the weathering characteristics of different patches.

Several studies have examined the weathering characteristics of limestone fault scarps. Wallace et al. (1984) was one of the first to qualitatively describe weathering differences between two slip patches on a fault scarp. Wallace et al. (1984) noted the difference between a lower ~3 m of fresh scarp exposed in the 1915 Pleasant Valley earthquake and that of an upper more lichen-covered, rougher, and more heavily solution-pitted band. Stewart (1996) measured the surface roughness of the Kaperelli and Pisia faults in the eastern Gulf of Corinth, both of which ruptured to the surface and exposed fresh scarp faces in the 1981 Corinth earthquakes. Stewart's (1996) results showed that fault surfaces above the 1981 slip patches were generally rougher than the fresh exposure; however, because of the heteroscedasticity in the data, caution was urged in interpreting paleoseismic histories based on surface roughness beyond historical and MRE events. Mechernich et al. (2018) revisited this fault using a multi-proxy approach and identified 6-8 weathering bands (or stripes) that could be correlated with earthquakes. Tucker et al. (2011) found a positive correlation between pit depths and cosmogenic exposure-ages on the Magnola fault scarp in the central Apennines, Italy. Giaccio et al. (2003) used image analysis to identify previous bands of soil-bedrock contact on the Campo Felice fault in the same region. One of the best-established techniques for carbonate fault scarps has been the Rare Earth Element (REE) method. Manighetti et al. (2010) developed the technique on a fault of known earthquake history by examining peaks of REE+Y left over by soil weathering within the first 1.5 m of the ground surface. Mouslopoulou et al. (2011) and Mouslopoulou et al. (2014) were the first study to apply and subsequently confirm the technique on a fault of unknown paleoearthquake history in Crete.

Surface roughness from terrestrial laser scanning (TLS) microtopography data have also been used to investigate many aspects of fault friction (Sagy et al., 2007; Candela et al., 2009; Brodsky et al., 2016) and scarp weathering (Wei et al., 2013; Wiatr et al., 2015; He et al., 2016; Tye and Stahl, 2018). Many of these works have investigated the effects of weathering on the fractal distribution of scarp surface relief (Wei et al., 2013; He et al., 2016). The analysis of Wei et al. (2013) showed that the effects of weathering on scarp microtopography are most pronounced at spatial scales of several centimeters or less.

Zreda and Noller (1998) presented the first study using ^{36}Cl exposure-age dating on a limestone fault scarp in their research on the Hebgen fault in Montana, USA. In their study, they used relative weathering metrics (e.g. roughness, discoloration, pitting, and preservation of slickensides) as guides in grouping ^{36}Cl sample concentrations and apparent ages. Tye and Stahl (2018) re-evaluated the same exposure using the Schmidt hammer, adjusted Geological Strength Index (GSI), and TLS and found that R-values decreased in steps with increasing height on the scarp, which they attributed to incremental exposure of the scarp in 3-4 earthquakes. Interpretations of TLS data, however, were inconclusive, which could be partially attributed to the macro-scale weathering characteristics of the Hebgen fault site (Tye and Stahl., 2018). In order to further test the utility of Schmidt hammer and TLS in characterising carbonate fault scarps, we selected a site with less geomorphic and lithologic complexity.

Methods

Study site

Our study site is located in central Nevada, USA, within the actively extending Basin and Range province (Fig. 1). East-west directed extension in the Basin and Range is accommodated by a series of N-S oriented normal faults, forming a series of topographic ranges and adjacent valleys. The site is located on the Pearce section of the Pleasant Valley fault (Wallace et al., 1984) at the southwestern range front of the Tobin Range (Fig. 1). The elevation of the site is c. 1490 m; it has a mean annual temperature (30-year normal) of 9.5 °C and mean annual precipitation of 210 mm (data sourced from National Oceanic and Atmospheric Administration 30-year normals between 1981-2010 for Winnemucca Airport climate station, located 75 km to the North along Pleasant Valley). The lithology of the fault scarp is massive, grey dolomitic limestone of the Triassic Natchez Pass Formation (Page, 1935; Stewart and Carlson, 1976).

The Pleasant Valley fault last ruptured in an earthquake on October 2nd 1915. The seismological moment magnitude (M_{Ws}) of the earthquake is estimated to be M_{Ws} 6.9-7.0 but is uncertain due to the low number of recording seismograph stations near the epicenter (Doser, 1988). The geological moment magnitude (M_{Wg}, estimated from field observations of length and displacement) is significantly higher at M_{Wg} 7.3-7.5 (Wallace et al., 1984; Wesnousky, 2008; dePolo, 2013). One potential reason for this discrepancy is that the October 2nd earthquake was preceded, on the same day, by two significant foreshocks that could have caused surface rupture along sections of the Pleasant Valley fault; however, no historical account is definitive in identifying surface rupture from these events (Wallace et al., 1984; Doser, 1988; dePolo, 2013). Thus, for the purposes of this study, we assume that the observed displacement was accrued during a single event (the 1915 earthquake).

Displacement on the Pleasant Valley fault in 1915 was predominantly dip-slip with a small dextral component. Average net slip was 3.2-3.6 m, with average and maximum dip-slip values of 3 and 6.7 m, respectively (dePolo, 2013). Four fault sections have been defined on the basis of local geology, morphology, and trace continuity: (from north to south) the China Mountain, Tobin, Pearce, and Sou Hills sections. The Pearce section is the longest at ~30 km.

At the study site on the Pearce Section of the fault (Fig. 1B), the exposed fault plane strikes 185° and dips 50° to the West, with striae plunging 49° towards 295°, confirming predominantly dip-slip motion with a minor dextral component. The scarp is present as a single exposed fault plane for c. 7.5 m scarp height but becomes progressively covered in vegetation above 5 m. We observed no gouge on the surface. Wallace et al. (1984) reported dip-slip of 3 m in the 1915 earthquake at this location and noted bands with different weathering on the limestone scarp, with a transition zone 'a few centimeters wide' (pg. A23). We visually confirmed the observation of this transition zone between 1915 and pre-1915 slip patches, and that the upper patch had 0.5 cm deep and 1-2 cm wide solution pits, more intense lichen cover, and elongate rillenkarren. This upper weathered zone was attributed to a longer duration of weathering on the upper part of the scarp due to one or more pre-1915 earthquakes on the fault by Wallace et al. (1984); they proposed an age of several thousand, but less than 12,000 years, for this event.

Paleoseismic studies on the Pleasant Valley fault have not yielded conclusive evidence for the timing or amount of slip in prehistoric earthquakes. An exploratory trench across the scarp in alluvial fan gravels, ~18 km to the north from our site, found evidence for two or more pre-1915 events that were estimated to be Holocene-late Pleistocene in age (Bonilla et al., 1980). Another unpublished trenching study ~2.5 km to the south revealed evidence for several faulting events on a ~13 m high compound scarp, but no dateable material was recovered (Anderson and Machette, 2000).

Schmidt hammer methods

A mechanical N-type Schmidt hammer with an impact energy of 2.207 N m was used to test rebound values of the Pleasant Valley scarp. We followed the sampling protocol of Tye and Stahl (2018), whereby we recorded the first impact R-value and four subsequent values at each point along the scarp in order to calculate the R-value range, ΔR. This R-value differencing approach is used to account for small variabilities in rock mass properties that are inherent in any lithology. That is, even if first-impact R-values are significantly different on patches of equivalent exposure-age, ΔR may remain relatively stable (Tye and Stahl, 2018). We chose a sampling spacing of 10 cm in two c. 5 m-high scarp transects, as above this scarp height (i) vegetation obscured the upper ~2.5 m and (ii) we had no confidence in a single fault plane continuing beyond that point. The two transects were located approximately 10 m apart along the scarp. All samples were collected over a period of one day in dry conditions by the same operator. We avoided lichen cover and facets that appeared to be more freshly exposed than the surrounding scarp. We also avoided solution pits and attempted to sample on the flattest surface available at that height. Any chipping of the rock surface was noted and a new sample location was chosen at that same scarp height. In doing so, we aimed to test both the near-surface limestone 'hardness' and mm-scale (from the diameter of the contact point) surface roughness. The Schmidt hammer was calibrated on a test anvil before and after the trip to ensure no instrument degradation took place.

Terrestrial Laser Scanning (TLS) methods

In order to quantify cm-scale surface roughness and assess its spatial relationship with rupture patches corresponding to the 1915 and pre-1915 events, we analyzed terrestrial laser scanning (TLS) data collected from the Pleasant Valley scarp. TLS data were collected using a Riegl VZ1000 scanner from four scan positions with average point spacing of ~3 mm in the horizontal and vertical directions on the scarp face. TLS point data were colored using a Nikon D810 Full Frame digital camera mounted on the scanner. One scan position from each of the two study sites (northern and southern) was selected for further analysis and vegetation and irregular erosion features were removed from the data manually. For each scan position, points located on the fault surface were transformed such that the scarp face corresponded with the XY plane. Following this transformation, scarp-normal elevation values of the points were gridded with 3 mm grid resolution.

As a measure of surface roughness, we calculated topographic variance within a square moving window ~5 cm in width (after Tye and Stahl, 2018). Within each window, the gridded data were fit to a best-fit fault plane (to account for slight changes in surface orientation across the scarp), and the variance of the residuals were calculated. The ~5 cm moving window moved in ~2.5 cm increments, such that half the gridded data were shared between adjacent windows. Finally, for selected transects at each study site, topographic variance values were horizontally averaged and plotted against scarp height in 2.5 cm increments to visualize any vertical trends within the data.

Curve-fitting

We followed the same procedure outlined in Tye and Stahl (2018) for curve-fitting scarp height versus ΔR and TLS-derived roughness data and model selection, and refer the reader there for details of the method. We conducted curve-fitting with natural log-transformed data to reduce effects of heteroscedasticity. Linear, power-law, and step-function models were considered as candidate models. Theoretically, a fault scarp incrementally exposed in earthquakes should have stepped ΔR and roughness versus scarp height relationships, but with unknown amounts and locations of steps. Best-fitting parameters were determined via pattern search for linear and power-law modes (Hooke and Jeeves, 1961) and via brute force maximum likelihood for the stepwise models. For the latter, we did not specify the number of steps or their locations, allowing the algorithm to identify these parameters automatically. We used the Bayesian Information Criterion (BIC; Schwarz, 1978) to compare model goodness-of-fit while penalising for additional model parameters. The lowest BIC values indicate a balance between model fit and number of parameters, and therefore point towards the preferred model.

Results

Schmidt hammer

Schmidt hammer R-values generally decrease with subsequent impacts in both transects (Fig. 2). At 85% of the sample locations, first or second impact R-values (R_1 and R_2) were the lowest, and fourth or fifth impact R-values (R_4 and R_5) were the highest. There is some alignment of ‘peaks’ and ‘troughs’ between sample sites that affect all R-values (Fig. 2). Minimum and maximum R-values both decrease with increasing height on the scarp, though the decrease is more pronounced in R-value minima (Fig. 2). Between ~2.25 m and 3 m in both transects, the difference between R-value minima and maxima (ΔR) starts to become larger by 8-10 points on average. The standard deviation of ΔR also becomes larger above this scarp height, increasing from σ=2.2 to σ=4.8. This area approximately coincides with the transition zone of weathering patterns, identified visually, between 1915 and pre-1915 slip patches (Fig. 2).

BIC values were calculated using $\sigma_{\ln(\Delta R)} = 0.4$, which is representative of the scatter of ln(ΔR) values within the inferred 1915 and pre-1915 slip patches (Table 1). Use of $\sigma_{\ln(\Delta R)}$ values of 0.3 to 0.5, encompassing the full range of local scatter in ln(ΔR) values, did not change the preference for a stepwise model. Of the four model fits considered for each transect (Figs. 3 and 4), the stepwise functions yield the lowest BIC values despite having a larger number of parameters constraining the fit. There is a slight preference for the one-step model in both transects (Table 1). The best-fitting step location for the northern transect is at 2.7 m (Table 1; Fig. 3C), 30 cm below where we had visually identified the cut-off between transition zone and pre-1915 scarp (Fig. 2B). The best-fitting step location for the southern transect is located at 2.2 m (Table 1; Fig. 4C), which is at the boundary of the 1915 slip patch and transition zone above (Fig. 2A).

TLS

Our TLS data quantify cm-scale roughness variations over the surface of the fault scarp (Fig.5). Visual distinctions between the 1915 and pre-1915 event rupture patches are present in the colored point clouds (Fig. 5 a, d). Though lighting was different between the sites, the pre-1915 event rupture patch is darker and appears more pitted than the 1915 event rupture patch at both the northern and southern sites (Fig. 5 a, d). Measurements of topographic variance within a ~5 cm footprint also suggest a measurable difference in surface roughness at this scale between the 1915 and pre-1915 event rupture patches (Fig. 5 b, e). The pre-1915 event rupture patch is rougher than the 1915 event patch, and the boundary between the two rupture patches corresponds with the boundary suggested by visual inspection of the scarp point clouds (Fig. 5 a, d) and field observations. Horizontally averaged roughness values suggest a stepwise pattern in which the 1915 and pre-1915 event rupture patches have uniform roughness values that are distinct from one another (Fig. 5 c, f).

We use BIC to assess the most appropriate functional form to fit the horizontally averaged roughness data (Table 2), using a similar set of functions as tested for the Schmidt hammer data. In the cases of both the northern and southern sites, BIC values indicate that there is a positive to strong preference for a stepwise functional form with one break (Fig. 5c ,f; Table 2). The stepwise model with one break indicates the values of topographic variance that characterize the 1915 and pre-1915 rupture patches at the northern and southern sites. At the northern site (Fi. 5 a-c), the pre-1915 rupture patch has a topographic variance value (over a ~5 cm wavelength) of about $e^{-13.5}$, whereas the 1915 rupture patch has a topographic variance value of about $e^{-14.5}$ (Fig. 5c).- At the southern site (Fig. 5 d-f), the pre-1915 rupture patch has a topographic variance of about $e^{-14.3}$ and the 1915 rupture patch has a value of about $e^{-15.2}$ (Fig. 5f). -Thus, in both cases, measured roughness values are a factor of ~*e* greater in the pre-1915 rupture patch than in the 1915 rupture patch.

Discussion

Preferred model and demarcation of single event displacements (SEDs)

Visual inspection, Schmidt hammer R-values and topographic variance (henceforth referred to as TLS-derived surface roughness) all detect a contrast between 1915 and pre-1915 slip patches, while the exact characteristics of the transition zone between the two are less clear. Visually (Fig. 2), the upper (pre-1915) patch appears rougher, more lichen covered, and 'rustier' in color than the transition zone. The transition zone is lichen free, but rougher and darker in color than the 1915 slip patch (Fig. 2).

The difference between R-value minima and maxima, or ΔR, increases from 1915 to pre-1915 patches (Figs. 3 and 4), which is consistent with previous interpretations that older patches are rougher and softer due to subaerial weathering (Tye and Stahl, 2018). The transition zone between the two slip patches has a variable ΔR signature in the two transects. In the northern transect, ΔR values gradually increase up-scarp within the transition zone to 3 m scarp height (Fig. 2B). The upper and lower boundaries of the transition zone are in fact approximated in the stepwise model with two steps (Table 1; Fig. 3D). In the southern transect, the ΔR boundary between 1915 slip patch and the transition zone is more abrupt (Figs. 2A & 4C). This is where the best-fitting stepwise model (using BIC) places the step (Table 1; Fig. 3C).

TLS-derived surface roughness has several implications for the processes controlling fault scarp surface roughness at the cm-scale. Horizontally averaged roughness values show a uniform distribution within the 1915 and pre-1915 event rupture patches with a significant difference in roughness between the two rupture patches (Fig. 5 c, f). This distribution of roughness indicates that the dominant control on surface roughness of the Pleasant Valley scarp is whether a particular ~5 cm patch of the scarp was exposed during the 1915 or pre-1915 event. The paleoseismic control on surface roughness conforms to field observations from the Pleasant Valley site and prior studies of other bedrock normal fault scarps, which also reveal approximately stepwise surface roughness distributions (Wiatr et al., 2015; He et al., 2016). Overall, our TLS data indicate that the Pleasant Valley scarp contains two regions of distinct roughnesses that in general correspond to the 1915 and pre-1915 event rupture patches.

A gradual transition is observed between the ΔR and TLS-derived roughness 'steps' between the 1915 and pre-1915 event rupture patches (Figs. 2-5). At both sites, the transitions occur over a band of 0.25 – 0.5 m scarp height. The transition is similar to that observed in other studies of fault scarp surface roughness, which has been hypothesized to reflect weathering within soil at the base of an exposed scarp between earthquakes (discussion below). The interpretation of these transition zones and locations of these steps is significant for estimating single event displacements (SEDs). We consider the transition zone to represent the region where soil or colluvium was in contact with the fault scarp prior to the 1915 earthquake. Identification of similar discolored bands have been identified on other fault scarps (e.g. Giaccio et al., 2003; Mechernich et al., 2018). It follows that these bands will be more weathered than the subsurface fault scarp, and depending on the length of time (i.e. recurrence interval of faulting), soil chemistry, and colluvium or soil density, they will exhibit weathering characteristics consistent with the previously exposed patch (e.g., our southern transect) or transitional between the two patches (e.g., our northern transect). The fact that the zones do not follow one particular ΔR pattern leads to uncertainty in determining how much the fault slipped in previous earthquakes.

Visually, we would estimate an SED of between 2.2-3.0 m of dip slip of the Pleasant Valley in 1915 at the two transect sites, whereas we would estimate between 2.2 (Fig. 4c) and 2.9 m (Fig. 5f) for the southern transect, and 2.7 and 3.6 m for the northern transect, based on curve fits to ΔR and TLS-derived surface roughness, respectively (step location values from Tables 1 and 2). The difference between the two sites and the two techniques can be attributed to undulations in the elevation of the colluvium at the base of the scarp, the scale of roughness being measured, and the varying properties of the transition zone. Averaging our four step locations, we would estimate dip slip SED of 2.85 m, which is in decent agreement with the 3 m dip at the site (Wallace et al., 1984) and our visual inspection. We see no evidence for more than one rupture patch in the 2-3 m of fault scarp preserved above the transition zone, so we would estimate a minimum SED of ≥2-3 m for the penultimate event at this site. We cannot rule out small, closely-spaced events older than the 1915 slip patch, but there is no evidence for this in our data or in the historic record.

Sources of uncertainty in determining SEDs

Using this method, sources of uncertainty in determining SEDs include

(i) Inherent heterogeneity in limestone lithology and surface weathering, leading to natural variability in ΔR or TLS-derived surface roughness values,;

(ii) Natural variability in Schmidt Hammer R-Values due to instrumental error,;

(iii) Epistemic uncertainty regarding small displacement events, events closely spaced in time, or non-tectonic modification to the scarp's exposure history,;

(iv) The presence of a 'transition zone' between patches and locations of best-fitting model step within it.;

While (i) (ii) and (iii) are unable to be completely eliminated, these forms of uncertainty can be reduced by careful site selection and sample design. Point (iiv) warrants further discussion below.

The transition zone can take on weathering characteristics, measured by -ΔR values, of the older slip patch *or* of both patches. In this study, the best-fitting model for Schmidt hammer data either places a step near the top or bottom of this zone. This leads to differences in estimated SED values between transects, using only the Schmidt hammer data, of ~0.5 m and an underestimation of the SED in our curve fitting of between 0.3-0.8 m (~10-27%) for the most recent event. On other fault scarps, depending on how these transition zones weather, their thicknesses, and whether they are present at all, this effect may lead to over- or underestimation of SEDs on older patches using the Schmidt hammer. There is not a general solution to this problem, as varying weathering rates; soil density, thickness, and chemistry; and limestone properties will influence how these zones weather in different settings. However, TLS-derived surface roughness data place the step higher (i.e. nearer the top of the transition zone) in both transects, therefore providing a counterbalance to the finer-scale surface roughness and/or surface hardness measured by the Schmidt hammer.

Application to other limestone fault scarps – where can this be used and how can it be improved?

This study demonstrates unambiguously that TLS and the Schmidt Hammer are useful for demarcating SEDs associated with the most recent paleoearthquakes on carbonate fault scarps provided certain tectonic, climatic, and lithologic conditions are met. The Pleasant Valley fault is a low slip rate fault with a long recurrence interval of surface rupturing earthquakes, which means that previously exposed slip patches have a long time (10^3-10^4 years) to weather prior to exposure of the next patch. Thus, limestone from the penultimate event patch has time to develop pits, rillenkarren, and surface rinds that will distinguish itfrom the relatively fresh limestone of the most recent event patch. Under similar low weathering rate conditions, differences in ΔR may not be statistically distinguishable if recurrence intervals are shorter than 10^3 years (e.g., Tye and Stahl, 2018).

The other factor that influences where this method can be applied is highlighted by the scale of SEDs relative to that of near-surface weathering (i.e. transition zone thickness). The Pleasant Valley fault has 2-3 m scale displacements and a transition zone of ~0.5 m, leading to uncertainties of ~20% in models of SEDs. If the transition zone thickness was smaller, or the displacement larger, this uncertainty would be reduced. Where transition zone locations are unable to be established independently, small ratios of SED to transition zone thickness will limit the utility of the Schmidt Hammer method.

Weathering rates will also influence where this technique can be applied. Because weathering rates typically decrease with exposure age (e.g. via a power law or similar curvilinear trends; e.g., Stahl et al., 2013), all of the oldest slip patches will have similar weathering characteristics beyond a certain age. Additionally, older slip patches may begin to physically weather such that a continuous fault plane is no longer recognizable; in this instance, the hardness and/or cm-scale roughness may be more indicative of the presence of macro-scale fractures rather than time-dependent chemical and biokarstic weathering (e.g., Giaccio et al, 2003). Significant post-exposure alteration via caliche (or calcrete) development is also likely to affect both Schmidt hammer and TLS-derived surface roughness measurements.

Targeting well-dated faults in different climates, with variable recurrence intervals and/or SEDs, will provide further evidence the Schmidt hammer and TLS can be used to demarcate slip patches. A multi-proxy approach that combines Schmidt hammer, TLS, and other (e.g., REE, photographic, seismic velocity) methods could also be used to reduce the uncertainty associated with any one technique. At present, combined Schmidt hammer and TLS seem to be of use for, at a minimum, characterising mm to cm-scale roughness contrasts between most recent and penultimate events. Further study of larger, multi-event scarps will confirm the climatic, tectonic, and lithologic conditions required for using this method to measure SEDs independently of historical or cosmogenic exposure age-dated events.

Conclusions

The weathering characteristics of two distinct slip patches on the Pleasant Valley fault scarp are evident in Schmidt hammer and TLS analysis. Our best fitting models to the ΔR and TLS data, using a Bayesian Information Criterion (BIC) places breaks between 1915 and pre-1915 slip patches at an average of 2.85 m on the scarp, which ~~works well~~is consistent with the reported and visually estimated ~3 m SED at the site. The presence of a weathering 'transition zone' between 1915 and pre-1915 patches is one major source of uncertainty, and handling of this uncertainty in other locations will depend on site-specific climate, lithologic, and soil properties. The penultimate event on the Pleasant Valley fault had an SED of ≥2-3 m, since there is no evidence of more than one event preserved above the transition zone in both Schmidt hammer and TLS data. We propose that a multi-proxy approach, incorporating our TLS and Schmidt hammer methods alongside other established techniques, might allow for even more robust SED estimates on multi-event bedrock fault scarps.

Acknowledgments

The authors would like to thank Nathan Niemi, Marin Clark, Eric Portenga, Kendra Murray and other members of the SCALE Lab at the University of Michigan for providing valuable discussion in developing this method. We would like to thank Proceq USA for kindly allowing us to test the Pundit 200 and Pulse Echo for this purpose. Stahl was supported by NSF EAR Fellowship 1451466. We thank Brendan Hodge for assistance with TLS data collection and reduction. This material is based on data, equipment, and engineering services provided by the UNAVCO Facility with support from the National Science Foundation (NSF) and National Aeronautics and Space Administration (NASA) under NSF Cooperative Agreement No. EAR-0735156. Two anonymous reviewers greatly improved the quality of the manuscript.

References

Anderson RE, Machette MN (compilers). 2000. Fault number 1136c, Pleasant Valley fault zone, Pearce section. Quaternary fault and fold database of the United States: U.S. Geological Survey website, https://earthquakes.usgs.gov/hazards/qfaults, accessed 11/02/2018 06:15 PM.

Aydin A. 2009. ISRM Suggested method for determination of the Schmidt hammer rebound hardness: Revised version. International Journal of Rock Mechanics and Mining Sciences **46**: 627-634. DOI: https://doi.org/10.1016/j.ijrmms.2008.01.020

Benedetti L, Finkel R, Papanastassiou D, King G, Armijo R, Ryerson F, Farber D, Flerit F. 2002. Post-glacial slip history of the Sparta fault (Greece) determined by 36Cl cosmogenic dating: Evidence for non-periodic earthquakes. Geophysical Research Letters **29**: 87-1-87-4. DOI: doi:10.1029/2001GL014510

Benedetti LC, van der Woerd J. 2014. Cosmogenic Nuclide Dating of Earthquakes, Faults, and Toppled Blocks. Elements **10**: 357-361. DOI: 10.2113/gselements.10.5.357

Benedict JB. 1985. Arapaho Pass, Glacial Geology and Archaeology at the Crest of the Colorado Front Range, Research Report No. 3: Ward, CO; Center for Mountain Arachaeology, 197.

Bonilla MG, Villalobos HA, Wallace RE. 1980. Exploratory trench across the Pleasant Valley fault, Nevada. U.S. Geological Survey Open-File Report 80–1245, 34 p., 1 plate.

Bosi C, Galadini F, Messina P. 1993. Neotectonic significance of bedrock fault scarps: case studies from the Lazio-Abruzzi Apennines (central Italy). Zeitschrift fur Geomorphologie, Supplementband **94**: 187-206

Breysse D. 2012. Nondestructive evaluation of concrete strength: An historical review and a new perspective by combining NDT methods. Construction and Building Materials **33**: 139-163. DOI: https://doi.org/10.1016/j.conbuildmat.2011.12.103

British Standard Testing Concrete. 1990. Recommendations tor the measurement of dynamic modulus of elasticity BS1881. Part 209.

Brodsky EE, Kirkpatrick JD, Candela T. 2016. Constraints from fault roughness on the scale-dependent strength of rocks. Geology 44: 19-22. DOI: 10.1130/g37206.1

Bull WB. 1996. Prehistorical earthquakes on the Alpine fault, New Zealand. Journal of Geophysical Research: Solid Earth **101**: 6037-6050. DOI: 10.1029/95JB03062

Candela T, Renard F, Bouchon M, Brouste A, Marsan D, Schmittbuhl J, Voisin C. 2009. Characterization of Fault Roughness at Various Scales: Implications of Three-Dimensional High Resolution Topography Measurements. Pure and Applied Geophysics 166: 1817-1851. DOI: 10.1007/s00024-009-0521-2

Colman SM, Dethier DP. 1986. Rates of Chemical Weathering of Rocks and Minerals. Academic Press: Orlando, FL; 603.

Crook R, Gillespie AR. 1986. Weathering rates in granitic boulders measured by P-wave speeds. In Rates of Chemical Weathering of Rocks and Minerals, Colman SM, Dethier DP (eds). Academic Press: Orlando, FL; 395–417.

Demirdag S, Yavuz H, Altindag R. 2009. The effect of sample size on Schmidt rebound hardness value of rocks. International Journal of Rock Mechanics and Mining Sciences **46**: 725-730. DOI: https://doi.org/10.1016/j.ijrmms.2008.09.004

dePolo C. 2013. Magnitude Values Used for M≥6 Earthquakes in Earthquakes in Nevada: 1840s to 2010. Nevada Bureau of Mines and Geology Open-File Report 13-7, NBMG Map 179.

Doser DI. 1988. Source parameters of earthquakes in the Nevada Seismic Zone, 1915–1943. Journal of Geophysical Research: Solid Earth **93**: 15001-15015. DOI: 10.1029/JB093iB12p15001

Fort R, Alvarez de Buergo M, Perez-Monserrat EM. 2013. Non-destructive testing for the assessment of granite decay in heritage structures compared to quarry stone. International Journal of Rock Mechanics and Mining Sciences **61**: 296-305. DOI: https://doi.org/10.1016/j.ijrmms.2012.12.048

Giaccio B, Galadini F, Sposato A, Messina P, Moro M, Zreda M, Cittadini A, Salvi S, Todero A. 2003. Image processing and roughness analysis of exposed bedrock fault planes as a tool for paleoseismological analysis: results from the Campo Felice fault (central Apennines, Italy). Geomorphology **49**: 281-301. DOI: https://doi.org/10.1016/S0169-555X(02)00191-5

Goudie AS. 2006. The Schmidt Hammer in geomorphological research. Progress in Physical Geography: Earth and Environment **30**: 703-718. DOI: 10.1177/0309133306071954

Hanks TC, Bucknam RC, Lajoie KR, Wallace RE. 1984. Modification of wave-cut and faulting-controlled landforms. Journal of Geophysical Research: Solid Earth 89: 5771-5790. DOI: 10.1029/JB089iB07p05771

He H, Wei Z, Densmore A. 2016. Quantitative morphology of bedrock fault surfaces and identification of paleo-earthquakes. Tectonophysics **693**: 22-31. DOI: https://doi.org/10.1016/j.tecto.2016.09.032

Hooke R, Jeeves TA. 1961. Direct search solution of numerical and statistical problems. Journal of the ACM 8: 212–229.

Laustela M, Egli M, Frauenfelder R, Kääb A, Maisch M, Haeberli W. 2003. Weathering rind measurements and relative age dating of rockglacier surfaces in crystalline regions of the eastern Swiss Alps. In Permafrost. Proceedings of the Eighth International Conference on Permafrost, July 2003, Phillips M, Springman S, Arenson L (eds). Swets and Zeitlinger (Lisse): Zurich; 627–632.

Maizels JK. 1989. Differentiation of late Pleistocene terrace outwash deposits using geomorphic criteria: Tekapo valley, South Island, New Zealand. New Zealand Journal of Geology and Geophysics **32**: 225-241. DOI: 10.1080/00288306.1989.10427585

Manighetti I, Boucher E, Chauvel C, Schlagenhauf A, Benedetti L. 2010. Rare earth elements record past earthquakes on exhumed limestone fault planes. Terra Nova 22: 477-482. DOI: 10.1111/j.1365-3121.2010.00969.x

Matthews JA, Owen G. 2008. Endolithic lichens, rapid biological weathering and schmidt hammer R-values on recently exposed rock surfaces: Storbreen glacier foreland, Jotunheimen, Norway. Geografiska Annaler: Series A, Physical Geography **90**: 287-297. DOI: 10.1111/j.1468-0459.2008.00346.x

McCarroll D. 1987. The Schmidt hammer in geomorphology: five sources of instrument error. BGRG Technical Bulletin 36: 16–27.

McCarroll D. 1991. The schmidt hammer, weathering and rock surface roughness. Earth Surface Processes and Landforms **16**: 477-480. DOI: doi:10.1002/esp.3290160510

Mechernich S, Schneiderwind S, Mason J, Papanikolaou ID, Deligiannakis G, Pallikarakis A, Binnie SA, Dunai TJ, Reicherter K. 2018. The Seismic History of the Pisia Fault (Eastern Corinth Rift, Greece) From Fault Plane Weathering Features and Cosmogenic 36Cl Dating. Journal of Geophysical Research: Solid Earth 123: 4266-4284. DOI: doi:10.1029/2017JB014600

Mouslopoulou V, Moraetis D, Benedetti L, Guillou V, Bellier O, Hristopulos D. 2014. Normal faulting in the forearc of the Hellenic subduction margin: Paleoearthquake history and kinematics of the Spili Fault, Crete, Greece. Journal of Structural Geology 66: 298-308. DOI: https://doi.org/10.1016/j.jsg.2014.05.017

Mouslopoulou V, Moraetis D, Fassoulas C. 2011. Identifying past earthquakes on carbonate faults: Advances and limitations of the ‘Rare Earth Element’ method based on analysis of the Spili Fault, Crete, Greece. Earth and Planetary Science Letters 309: 45-55. DOI: https://doi.org/10.1016/j.epsl.2011.06.015

Naik T, Malhotra V. 2003. The ultrasonic pulse velocity method. V. Malhotra, N. Carino (Eds.), Handbook on nondestructive testing of concrete, CRC Press, Florida: 179.

Nicol A, Walsh J, Berryman K, Villamor P. 2006. Interdependence of fault displacement rates and paleoearthquakes in an active rift. Geology 34: 865-868. DOI: 10.1130/g22335.1

Niedzielski T, Migoń P, Placek A. 2009. A minimum sample size required from Schmidt hammer measurements. Earth Surface Processes and Landforms **34**: 1713-1725. DOI: doi:10.1002/esp.1851
Page BM. 1935. Basin-Range Faulting of 1915 in Pleasant Valley, Nevada. The Journal of Geology **43**: 690-707
Sagy A, Brodsky EE, Axen GJ. 2007. Evolution of fault-surface roughness with slip. Geology 35: 283-286. DOI: 10.1130/g23235a.1
Sak PB, Fisher DM, Gardner TW, Murphy K, Brantley SL. 2004. Rates of weathering rind formation on Costa Rican basalt11Associate editor: E. H. Oelkers. Geochimica et Cosmochimica Acta **68**: 1453-1472. DOI: https://doi.org/10.1016/j.gca.2003.09.007
Schlagenhauf A, Gaudemer Y, Benedetti L, Manighetti I, Palumbo L, Schimmelpfennig I, Finkel R, Pou K. 2010. Using in situ Chlorine-36 cosmonuclide to recover past earthquake histories on limestone normal fault scarps: a reappraisal of methodology and interpretations. Geophysical Journal International **182**: 36-72. DOI: doi:10.1111/j.1365-246X.2010.04622.x
Schwarz G. 1978. Estimating the dimension of a model. Annals of Statistics 6: 461–464.
Shakesby RA, Matthews JA, Owen G. 2006. The Schmidt hammer as a relative-age dating tool and its potential for calibrated-age dating in Holocene glaciated environments. Quaternary Science Reviews **25**: 2846-2867. DOI: https://doi.org/10.1016/j.quascirev.2006.07.011
Stahl T, Winkler S, Quigley M, Bebbington M, Duffy B, Duke D. 2013. Schmidt hammer exposure-age dating (SHD) of late Quaternary fluvial terraces in New Zealand. Earth Surface Processes and Landforms **38**: 1838-1850. DOI: doi:10.1002/esp.3427
Stewart I. 1996. A rough guide to limestone fault scarps. Journal of Structural Geology **18**: 1259-1264. DOI: https://doi.org/10.1016/S0191-8141(96)00049-1
Stewart JH, Carlson JE. 1976. Geologic map of north-central Nevada. Nevada Bureau of Mines and Geology Map **50**, 1:250,000.
Sumner P, Nel W. 2002. The effect of rock moisture on Schmidt hammer rebound: tests on rock samples from Marion Island and South Africa. Earth Surface Processes and Landforms **27**: 1137-1142. DOI: doi:10.1002/esp.402
Tesson J, Pace B, Benedetti L, Visini F, Delli Rocioli M, Arnold M, Aumaître G, Bourlès DL, Keddadouche K. 2016. Seismic slip history of the Pizzalto fault (central Apennines, Italy) using in situ-produced 36Cl cosmic ray exposure dating and rare earth element concentrations. Journal of Geophysical Research: Solid Earth 121: 1983-2003. DOI: 10.1002/2015jb012565
Török Á, Forgó LZ, Vogt T, Löbens S, Siegesmund S, Weiss T. 2007. The influence of lithology and pore-size distribution on the durability of acid volcanic tuffs, Hungary. Geological Society, London, Special Publications **271**: 251-260. DOI: 10.1144/gsl.sp.2007.271.01.24
Tucker GE, McCoy SW, Whittaker AC, Roberts GP, Lancaster ST, Phillips R. 2011. Geomorphic significance of postglacial bedrock scarps on normal-fault footwalls. Journal of Geophysical Research: Earth Surface **116**. DOI: doi:10.1029/2010JF001861
Tugrul A, Zarif IH. 2000. Engineering aspects of limestone weathering in Istanbul, Turkey. Bulletin of Engineering Geology and the Environment **58**: 191-206. DOI: 10.1007/s100640050075
Tye A, Stahl T. 2018. Field estimate of paleoseismic slip on a normal fault using the Schmidt hammer and terrestrial LiDAR: Methods and application to the Hebgen fault (Montana, USA). Earth Surface Processes and Landforms 43: 2397-2408. DOI: 10.1002/esp.4403
Wallace RE, Bonilla MG, Villalobos HA. 1984. Faulting related to the 1915 earthquakes in Pleasant Valley, Nevada. In *Professional Paper*.
Wei Z, He H, Shi F. 2013. Weathering history of an exposed bedrock fault surface interpreted from its topography. Journal of Structural Geology **56**: 34-44. DOI: https://doi.org/10.1016/j.jsg.2013.08.008
Wesnousky SG. 2008. Displacement and Geometrical Characteristics of Earthquake Surface Ruptures: Issues and Implications for Seismic-Hazard Analysis and the Process of Earthquake

Rupture. Bulletin of the Seismological Society of America **98**: 1609-1632. DOI: 10.1785/0120070111

Wiatr T, Papanikolaou I, Fernández-Steeger T, Reicherter K. 2015. Reprint of: Bedrock fault scarp history: Insight from t-LiDAR backscatter behaviour and analysis of structure changes. Geomorphology **237**: 119-129. DOI: https://doi.org/10.1016/j.geomorph.2015.02.019

Zreda M, Noller JS. 1998. Ages of Prehistoric Earthquakes Revealed by Cosmogenic Chlorine-36 in a Bedrock Fault Scarp at Hebgen Lake. Science **282**: 1097-1099. DOI: 10.1126/science.282.5391.1097

Table 1: Model fitting parameters for ln(ΔR) from the two fault transects. Lower values of BIC indicate more preferable models. One outlier ΔR value was removed from the northern transect at height=4.2 m.

	Northern Transect		**Southern Transect**	
Modelled ΔR-scarp height relationship	**BIC**	**Step location**	**BIC**	**Step location**
Linear	77.1	--	84.2	--
Power law	92.4	--	92.2	--
Stepwise (1 break)	**58.5**	**2.7 m**	**78.5**	**2.2 m**
Stepwise (2 break)	62.6	2.0 and 2.7 m	81.1	0.4 and 2.2 m

Table 2: BIC values for fits of different functional forms to the horizontally--averaged TLS-derived surface roughness data in Figure 5 c, f.

Modelled ln(variance)-scarp height relationship	Northern transect	Southern transect
Linear	577.0	539.2
Power law	758.8	610.0
Constant value	650.5	651.8
Stepwise (1 break)	**537.0 (step at 3.6 m)**	**535.9 (step at 2.9 m)**

Figure Captions

Figure 1: Location of the study site within (A) Basin and Range province of Nevada, USA, on the (B) Pearce Section of the Pleasant Valley fault In (B) the light colored band demarcated by red arrows is the surface rupture of the 1915 Pleasant Valley earthquake. The fault ruptured through both bedrock and unconsolidated alluvial fan gravels (C). The distinction between 1915 and pre-1915 slip patches is primarily color, which is determined by lichen cover (C & D).

Figure 2: Schmidt hammer rebound values (R-values) and orthophotography from the two transects, southern (A) and northern (B). Both transects are approximately 5 m long, measured on the fault plane from the point nearest the ground surface. Rebound values are colored by the order of five impacts (R_1-R_5) at each site spaced 0.1 m on the scarp. The difference between the maximum and minimum R-value at each site is called ΔR (see text for discussion). Striae are well-preserved on the lowest portions of the scarp exposed in the 1915 earthquake, and demonstrate predominantly dip slip motion. The patch above the 1915 rupture is lichen covered, but has small areas of bare rock suitable of Schmidt hammer testing.

Figure 3: The natural logarithm of ΔR plotted against scarp distance shows a general increase in ΔR with increasing height. For the northern transect, the best fitting model based on the Bayesian Information Criterion (BIC) is (C) – the stepwise model with one break at ~3 m.

Figure 4: The natural logarithm of ΔR plotted against scarp distance shows a general increase in ΔR with increasing height for the southern transect. The best-fitting model is (C) – a stepwise model with one break at ~2 m.

Figure 5: Terrestrial ~~lidar~~ laser scanning quantifies the surface roughness of the Pleasant Valley scarp. (a) TLS point cloud (shown in true color) collected from the northern study location at Pleasant Valley shows a sharp visual distinction between a relatively smooth and light-colored lower portion of the scarp associated with the 1915 event and an upper, relatively rough and darker-colored portion of the scarp. (b) Roughness (topographic variance) analysis was conducted over the entire point cloud. Inset shows roughness calculation procedure: a moving window moves over gridded TLS data, and within each moving window the variance in plane-normal elevation is calculated and plotted. The moving window is a square of ~5 cm dimension and moves ~2.5 cm between calculations, such that adjacent roughness calculations are based on window locations that share half their area. (c) Vertical variations in horizontally averaged roughness (variance) are plotted for a selected swath of data. Bold blue line indicates the mean ln(variance) for each row within the swath boundaries (shown by the rectangle in b), with error bars reflecting the standard deviation (1σ). Bold red line shows mean topographic variance within the 1915 event patch and the pre-1915 event patch. (d-e) are analogous to (a-c) but show data from the southern Pleasant Valley scarp study location.

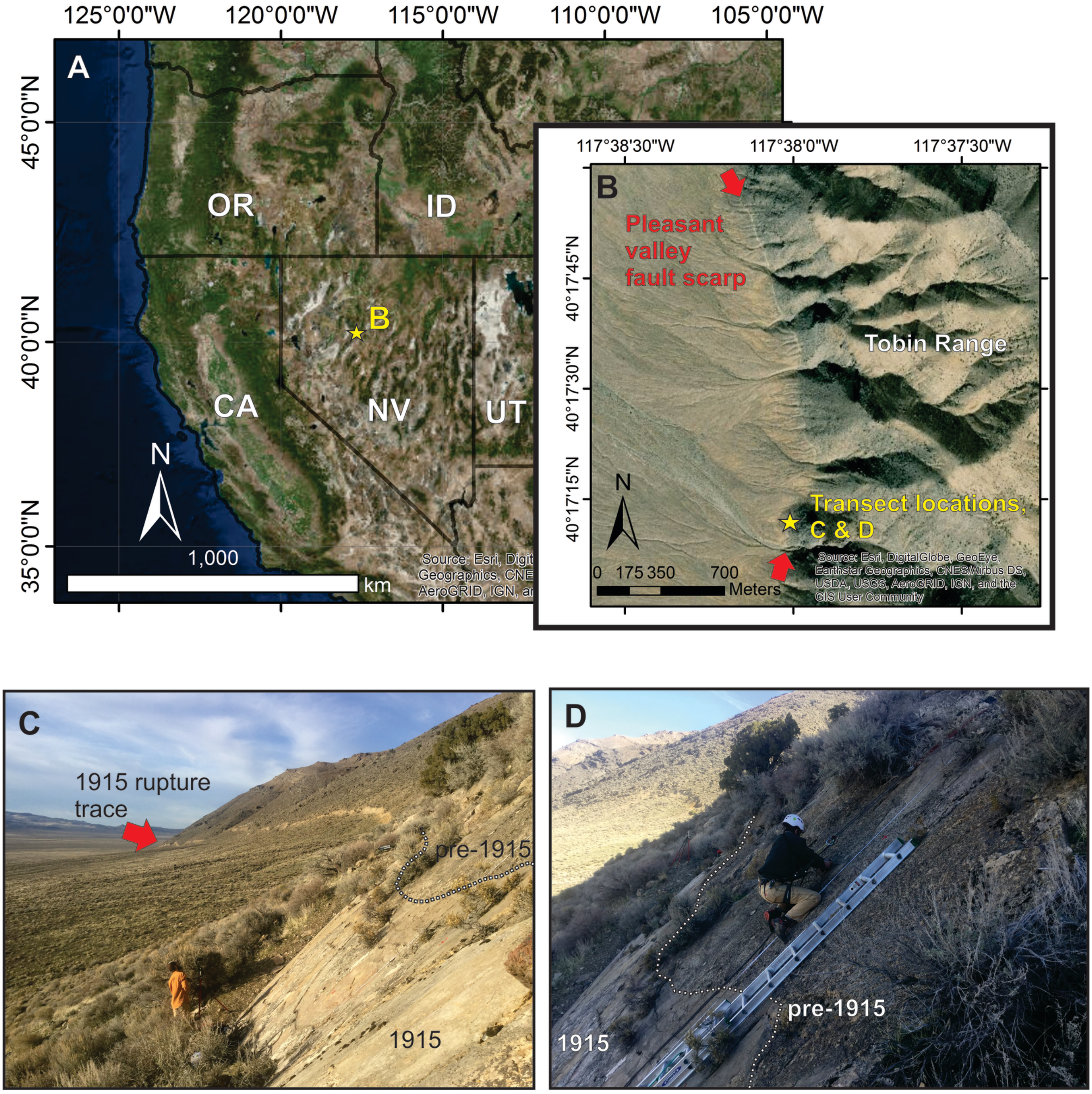

ESP_4748_F1_rev.tif

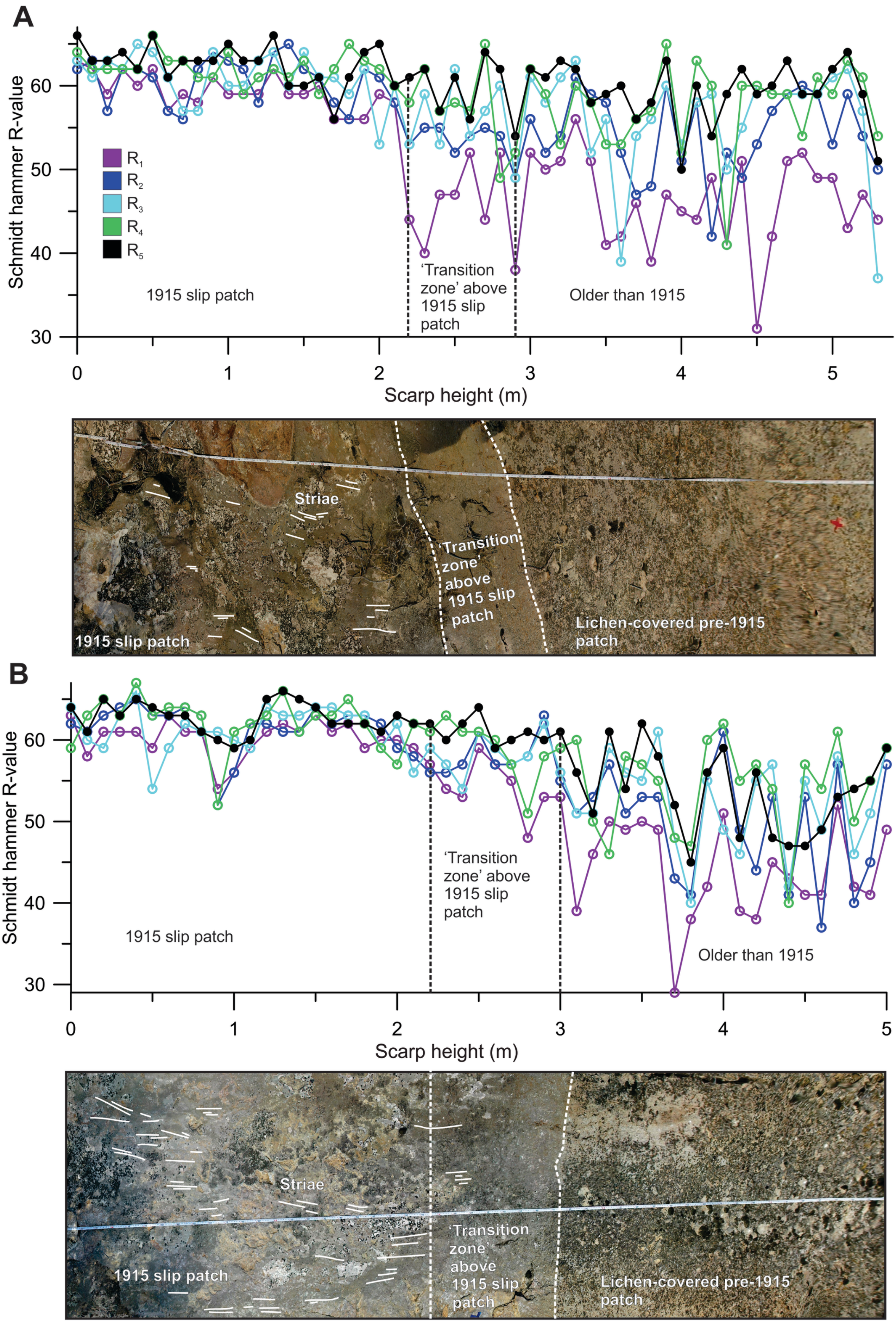

ESP_4748_F2_Rev.tif

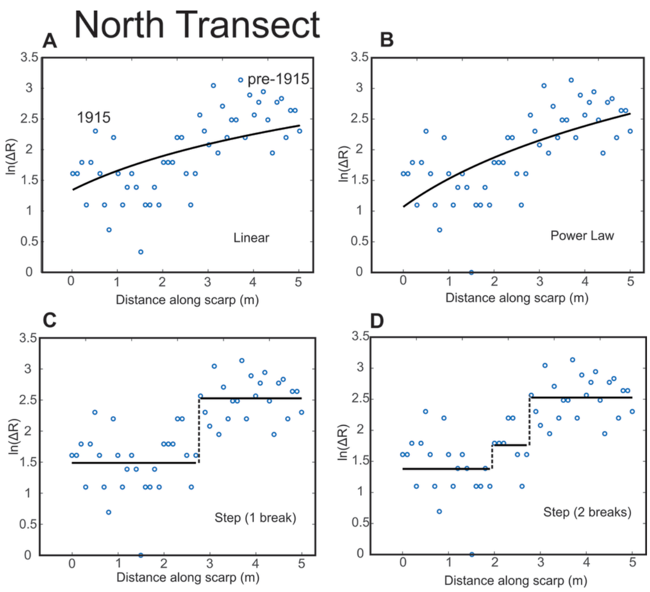

ESP_4748_F3.tif

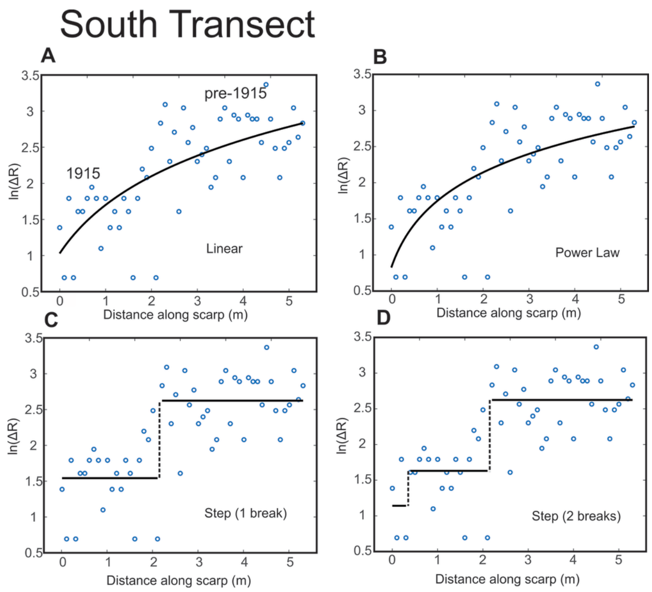

ESP_4748_F4.tif

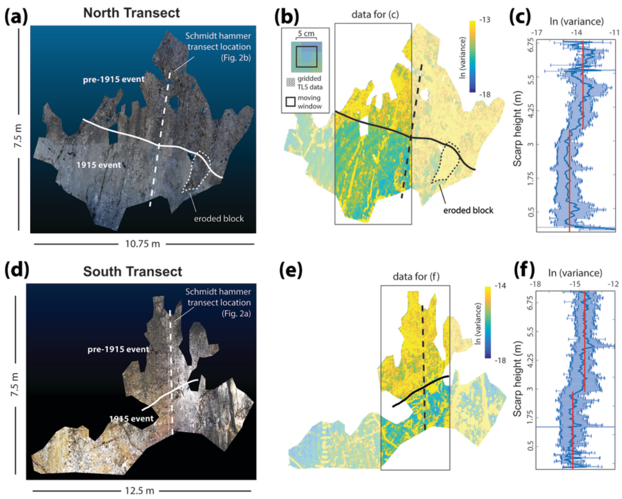

ESP_4748_F5_Final.tif